RSC Sustainability

ROYAL SOCIETY OF CHEMISTRY

PAPER

View Article Online
View Journal | View Issue

Cite this: *RSC Sustainability*, 2025, **3**, 3072

A novel cationic organic network for ultra-fast and high-capacity removal of toxic oxo-anions from water†

Yi-Shou Wang, * Xin-Yu Li, Rui-Rui Li, Xiao-Nan Yuan, Zhu-Qing Zhao and Xing-Xing Gou

Received 20th February 2025
Accepted 17th May 2025

DOI: 10.1039/d5su00122f

rsc.li/rscsus

Water pollution has become a global concern, especially from toxic metal-derived oxo-anions like CrO_4^{2-}, $Cr_2O_7^{2-}$, and TcO_4^-. Adsorption, particularly ion-exchange-driven adsorption, is a promising remediation approach. In this study, a novel imidazolium-based cationic organic network material, ImCON1, was designed and synthesised. Multiple characterisation techniques were used to analyse its structure and properties, including FTIR, solid-state ^{13}C CP-MAS NMR, SEM, TGA, XRD, and XPS. ImCON1 has a cross-linked, irregular spherical morphology, remarkable stability, and an amorphous nature. It shows high-efficiency removal of various toxic oxo-anions, CrO_4^{2-}, $Cr_2O_7^{2-}$, and MnO_4^- (as a surrogate for TcO_4^-) from water. The uptake capacities are 259 mg g^{-1} for CrO_4^{2-}, 1118 mg g^{-1} for $Cr_2O_7^{2-}$, and 694.5 mg g^{-1} for MnO_4^-, comparable to or higher than those of previously reported materials. The sorption kinetics follow the pseudo-second-order model, indicating rapid capture. ImCON1 is resistant to a wide pH range and effectively captures oxo-anions even in the presence of competing anions. An ImCON1-packed chromatographic column can efficiently remove oxo-anions from water through an anion exchange mechanism and can be reused for at least ten cycles. This novel cationic organic network material holds great promise for wastewater treatment applications and paves the way for developing high-performance adsorption materials at the molecular scale.

Sustainability spotlight

The synthesis of ImCON1, a novel cationic organic network, represents a significant sustainable advance. It enables ultra-fast and high-capacity removal of toxic oxo-anions from water. This aligns with the UN's Sustainable Development Goal 6 (Clean Water and Sanitation) by offering an efficient solution for wastewater treatment. With excellent pH resistance, good performance in the presence of competing anions, and reusability, it provides an environmentally friendly approach to purifying water and protecting aquatic ecosystems.

Introduction

In recent years, the escalating issue of water pollution has emerged as a global concern. The remediation of toxic pollutants present in water bodies has thus attracted significant attention on a worldwide scale.[1] Pollution stemming from metal-derived oxo-anions, such as CrO_4^{2-}, $Cr_2O_7^{2-}$, and TcO_4^-, has posed a pressing challenge due to their ubiquitous presence in the environment.[2–6] Notably, oxo-anions based on Cr(VI) have been demonstrated to exhibit highly carcinogenic and mutagenic properties concerning living systems.[7–11] In light of the significance of this issue, the U.S. Environmental Protection Agency (EPA) has incorporated such oxo-anions into the list of priority pollutants.[12] Various technologies have been developed for contaminant remediation, including adsorption, precipitation, and decomposition.[13–17] Among these, adsorption, particularly ion exchange-driven adsorption, is promising, demonstrating high efficiency and specificity in removing ionic contaminants from water.[18–20] Numerous materials have been developed and employed as sorbents, such as metal–organic frameworks (MOFs),[21–29] ion-exchange resins,[30] and porous hydrogels.[31] Nevertheless, the application of MOFs under harsh conditions is hampered by their poor stability, while resins are limited by their relatively low adsorption capacity and sluggish kinetics. In the case of porous hydrogels, their low cost, high specific surface areas, and considerable mechanical strength render them potential sorbents for water remediation. However, most reported porous hydrogels have exhibited moderate adsorption kinetics and capacity. Hence, developing adsorbents

Shaanxi Key Laboratory of Comprehensive Utilization of Tailings Resources, Shaanxi Engineering Research Center for Mineral Resources Clean & Efficient Conversion and New Materials, College of Chemical Engineering and Modern Materials, Shangluo University, Shangluo 726000, China. E-mail: 202138@slxy.edu.cn

† Electronic supplementary information (ESI) available. See DOI: https://doi.org/10.1039/d5su00122f

possessing high stability, excellent efficiency, and a straightforward fabrication process remains highly warranted.

Porous organic polymers (POPs)[32,33] and covalent organic frameworks (COFs)[34–37] are fabricated through strong covalent bonds, yielding high physicochemical stability. This remarkable stability has propelled them to the forefront of the domain of porous materials.[38–41] In real-time applications, it has been observed that stability is often prioritised over direct structure–property correlations. These compounds have attracted significant attention in various fields, such as gas adsorption, catalysis, and drug delivery.[42–45] However, their application in capturing hazardous oxo-anions from water is extremely scarce.[46] The fundamental prerequisite is a cationic network equipped with exchangeable anions to achieve anion capture *via* ion exchange. Cationic organic networks (CONs) represent a novel class of porous organic materials with significant potential for scavenging water contaminants. The organic skeletons within CONs enable facile structural design and modification. Meanwhile, the strong covalent bonds endow them with high-level stability even under harsh conditions.[47–55] More notably, the charged frameworks of CONs and abundant counterions can enhance adsorption performance. Various CONs have been developed and utilised to remove specific contaminants selectively.[56–62] However, research on CONs remains in its infancy, and the design of a single material with the capacity to adsorb a diverse range of water pollutants remains highly desirable. The charged active sites are unquestionably the most critical textural factor influencing the adsorption performance of a CON material. In light of this, we have endeavoured to optimise the efficiency of CONs by augmenting the density of charged sites. To this end, a novel imidazolium-based cationic organic network material, ImCON1 (Fig. 1a), was meticulously designed and synthesised. Subsequently, ImCON1 was employed to uptake diverse toxic oxo-anions present in water, and it exhibited a notably high adsorption capacity along with rapid kinetic behaviour.

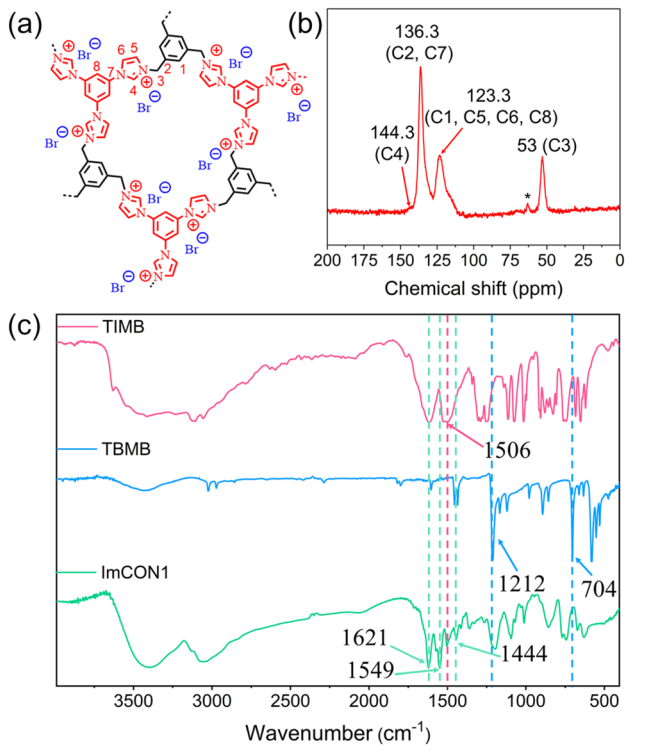

Fig. 1 (a) Structure of ImCON1, (b) solid-state ^{13}C CP-MAS NMR spectrum of ImCON1 (the peak marked with * is the spinning sideband), (c) FTIR spectrum of ImCON1 compared with monomers.

Results and discussion

Structural analysis

In the present study, the synthesis of ImCON1 was carried out through a quaternisation reaction between 1,3,5-tris(bromomethyl)benzene (TBMB) and 1,3,5-tris(imidazol-1-yl) benzene (TIMB) (Scheme S1†). Solid-state ^{13}C cross-polarized magic-angle spinning nuclear magnetic resonance (^{13}C CP-MAS NMR) was employed to investigate the chemical structure of ImCON1. As presented in Fig. 1b, the characteristic peak at 144.3 ppm (C4) corresponds to carbon atoms from the imidazolium rings, confirming the formation of intact ionic units within ImCON1. The peak at 53 ppm (C3) validates the benzylic methylene carbon attached to the imidazolium quaternary ammonium group. The carbons in benzene rings and those adjacent to the imidazolium N were identified at 136.3 and 123.3 ppm, respectively. These results suggest a quaternisation reaction of TBMB and TIMB.[63–67] These spectral assignments were cross-validated using Fourier transform infrared spectroscopy (FTIR) data. As depicted in Fig. 1c, the peaks at approximately 1212 cm^{-1} and 704 cm^{-1}, associated with the –CH_2 wagging in –CH_2Br groups and the C–Br stretching of TBMB, respectively, are undetected in ImCON1. The lack of these vibrational bands implies the successful reaction between TBMB and TIMB. The peaks at approximately 1615 and 1506 cm^{-1} are attributed to the C=C and C=N vibrations of imidazole moieties of TIMB. In ImCON1, these bands were red-shifted to around 1621 and 1549 cm^{-1}, respectively, indicating the existence of a quaternary ammonium group. The peak at approximately 1444 cm^{-1} in ImCON1 confirms the presence of the benzylic methylene group attached to the imidazolium quaternary ammonium group.

High-resolution scanning electron microscopy (SEM) images disclose the cross-linked, irregular spherical morphology of ImCON1 (Fig. 2a). The particle diameters of this material are approximately within the range of 1–1.5 μm. Thermogravimetric analysis (TGA) data suggested that ImCON1 possessed remarkable thermal stability (Fig. 2b). At temperatures exceeding 259 °C, a significant weight loss was observed, possibly due to the elimination of solvent molecules from the pores of ImCON1. The thermal degradation temperature of ImCON1 was approximately 417 °C. The X-ray diffraction patterns unequivocally confirm the amorphous nature of ImCON1, indicating the existence of a complex and disordered arrangement reminiscent of an ionic liquid-derived structure (Fig. S1†). The absence of long-range order implies that the framework comprises randomly packed particles instead of crystalline domains. However, the broad diffraction peaks at

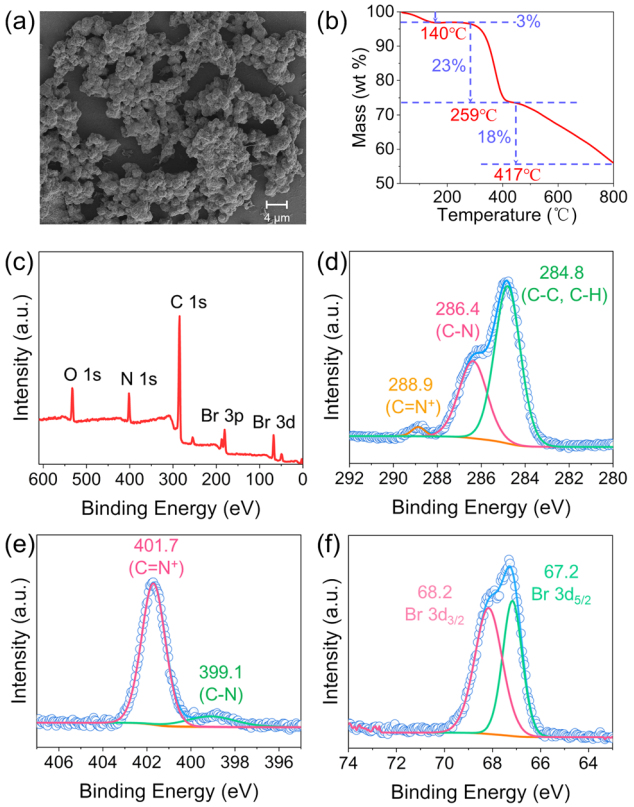

Fig. 2 (a) SEM image, (b) TGA curve, and XPS spectra of ImCON1 (c) survey, (d) C 1s, (e) N 1s and (f) Br 3d.

7.5° and 23.5° indicate that ImCON1 still preserves an organisation typical of ionic networks.

The chemical compositions of the ImCON1 materials were rigorously analysed *via* X-ray photoelectron spectroscopy (XPS). In the full survey spectra presented in Fig. 2c, five distinct peaks, located at 533.6 eV, 402 eV, 285.5 eV, 183 eV, and 68 eV, can be readily identified. These peaks correspond to O 1s, N 1s, C 1s, Br 3p, and Br 3d, respectively. The detection of oxygen (O) at 533.6 eV is attributed to water absorption, a finding that is consistent with the results from FTIR and TGA. This congruence among the different analytical techniques validates the reliability of the characterisation of the ImCON1 materials. Turning to the C 1s spectrum, as depicted in Fig. 2d, ImCON1 exhibits three well-defined peaks at binding energies (BE) of 284.8 eV, 286.4 eV, and 288.9 eV. These peaks signify the carbon species from aromatic rings, alkyl linkers, and the C=N$^+$ bonds within the imidazolium rings. The N 1s spectrum, shown in Fig. 2e, clearly elucidates the nitrogen composition. The dominant peak, with a relatively high BE value of 401.7 eV, represents the highly delocalised imidazolium cations (C=N$^+$). Conversely, the smaller peak, with a lower BE value of 399.1 eV, can be attributed to non-ionic nitrogen atoms within the imidazolium ring.[56] Regarding the Br 3d spectra, as presented in Fig. 2f, two prominent peaks centered at 67.2 eV ($3d_{5/2}$) and 68.2 eV ($3d_{3/2}$) are observed. These peaks confirm the successful incorporation of the targeted bromide anions paired with the imidazolium cations. Overall, the XPS data provide a comprehensive and in-depth understanding of the chemical constitution and bonding within the ImCON1 structure, thereby contributing to a more profound knowledge of the material's properties at the atomic and molecular levels.

To evaluate the performance of ImCON1 as an ion-exchange-based adsorbent, it was essential to understand its physical properties, including porosity, surface morphology, and the surface charge of the polymer. These parameters are crucial in determining the anion uptake performance of such materials in an aqueous medium. Low-temperature N_2 gas adsorption experiments (Fig. S2a†) were conducted to assess the porous properties. Before the gas uptake experiments, the ImCON1 sample was activated by heating it at 120 °C for several hours, followed by N_2 gas adsorption and desorption at 77 K. A notably low nitrogen uptake was recorded in the low relative pressure range (P/P_0 = 0–0.6). However, a gradual increase in N_2 uptake in the relatively high P/P_0 region indicated the presence of mesopores. Employing the BET isotherm model, the surface area of ImCON1 was determined to be 1.80 $m^2\ g^{-1}$. The pore size distribution calculated using nonlinear density functional theory (NL-DFT) demonstrated the microporous nature of ImCON1 (Fig. S2b†). The relatively low surface area resulted from substantial blockage of the internal voids/pores by the bromide counteranions associated with the cationic backbone of the as-synthesised ImCON1. Field emission scanning electron microscopy (FE-SEM) micrographs revealed an agglomerated morphology with evenly distributed elements (C, N, and Br), as demonstrated by energy-dispersive X-ray spectroscopy (EDX) mapping (Fig. S3†). The EDX data further verified the presence of bromide counteranions within the void spaces of ImCON1, which consequently led to a reduced specific surface area of the ionic ImCON1.

Adsorption performance

Since ImCON1 is a highly charged cationic framework featuring open apertures and large cavities, it exhibits potential for application in ion exchange processes involving anionic pollutants. To evaluate the adsorption properties of ImCON1, CrO_4^{2-} was initially selected as the target analyte for investigation. 3 mg of freshly synthesised ImCON1 sample was carefully placed into a 10 mL aqueous CrO_4^{2-} solution with an initial concentration of 0.17 mM contained within a glass vial. Subsequently, the adsorption kinetics were monitored *via* ultraviolet-visible (UV-vis) spectroscopy of the CrO_4^{2-} solution at predefined time intervals. Remarkably, as depicted in Fig. 3a, the intensities of the characteristic absorbance at λ_{max} = 372 nm diminished to zero within a mere 1 minute. The decline in the CrO_4^{2-} concentration was further corroborated by the visible colour transformation of the CrO_4^{2-} solution. As shown in the inset of Fig. 3a, the solution underwent a distinct colour change from yellow to colourless within just 1 minute. This can be ascribed to the ability of CrO_4^{2-} anions in the solution to permeate the voids of ImCON1 through ion exchange with bromide anions. Additionally, the colour of the powder suspended in the solution shifted from white to orange, which provides strong evidence that CrO_4^{2-} anions had been adsorbed

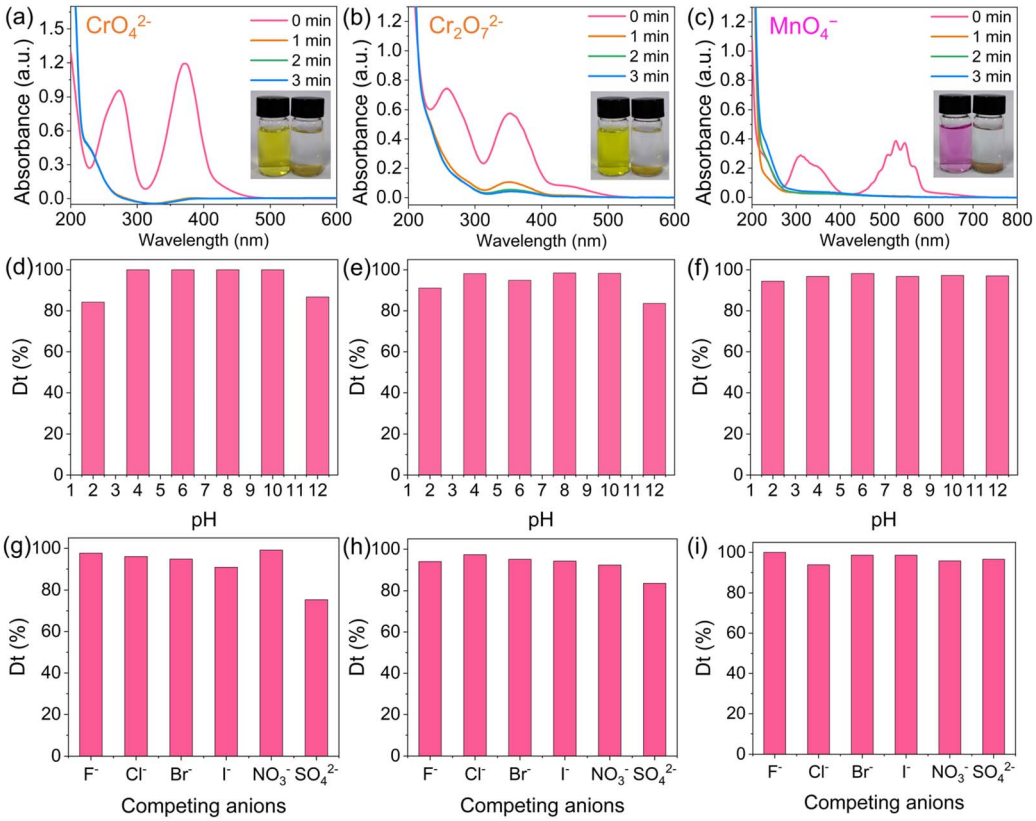

Fig. 3 UV-vis spectroscopy in the presence of ImCON1 at different time intervals for the water solution of (a) CrO_4^{2-}, (b) $Cr_2O_7^{2-}$ and (c) MnO_4^-; effect of pH value on the capture efficiency of (d) CrO_4^{2-}, (e) $Cr_2O_7^{2-}$ and (f) MnO_4^- by ImCON1; the bar diagrams represent the removal efficiency of ImCON1 in the presence of competing anions for (g) CrO_4^{2-}, (h) $Cr_2O_7^{2-}$ and (i) MnO_4^-.

into the samples. Furthermore, a new characteristic absorption band emerged at 942 cm^{-1}, attributable to the presence of CrO_4^{2-} anions, thus indicating that CrO_4^{2-} anions had supplanted bromide anions within the channels of ImCON1 (Fig. S4†). The kinetic data were fitted using the pseudo-second-order equation, yielding a kinetic constant (k_2) of 0.0343 g mg^{-1} min^{-1}, with a correlation coefficient $R^2 > 0.999$ (Fig. S7†). This result strongly suggests the rapid capture ability of the material towards CrO_4^{2-} ions. ImCON1 exhibited a high adsorption capacity of CrO_4^{2-} from aqueous solutions. The uptake capacity reached 259 mg g^{-1}. The adsorption capacity of CrO_4^{2-} is comparable to that of the recently reported adsorbents (Table S1†). To obtain the adsorption isotherm for CrO_4^{2-}, a series of aqueous K_2CrO_4 solutions with varying concentrations were employed. Subsequently, the experimental data were fitted to the Langmuir model (Fig. S10†).

A similar approach was adopted to study the capture of dichromate anion ($Cr_2O_7^{2-}$) from water. After exposing ImCON1 to an aqueous $Cr_2O_7^{2-}$ solution, the supernatant liquid transitioned from yellow to colourless. The characteristic peak of $Cr_2O_7^{2-}$ emerged at $\lambda_{max} = 350$ nm, and its absorbance was monitored for time-dependent studies (Fig. 3b). Within a 3 minute interval, approximately 96% of the $Cr_2O_7^{2-}$ was removed from the water. Simultaneously, the white ImCON1 gradually turned yellow. A novel characteristic absorption band manifested at 940 cm^{-1}. This can be ascribed to the presence of $Cr_2O_7^{2-}$. This indicates that $Cr_2O_7^{2-}$ had replaced bromide anions within the channels of ImCON1, as presented in Fig. S5.† Subsequently, the kinetic data were subjected to fitting using the pseudo-second-order equation. The kinetic constant k_2 was determined to be 0.009 g mg^{-1} min^{-1}, with a correlation coefficient $R^2 > 0.999$ (Fig. S8†). To the best of our knowledge, this kinetic constant is significantly higher than those of most reported adsorbents, which indicates the rapid adsorption property of ImCON1 towards $Cr_2O_7^{2-}$. Furthermore, the capacity of ImCON1 for $Cr_2O_7^{2-}$ ions was calculated (1118 mg g^{-1}) from the UV-vis study. Notably, this value surpasses the capture capacities of most of the adsorbent materials reported in the existing literature (Table S2†), suggesting that ImCON1 can function as an efficient adsorbent. The adsorption isotherm was acquired to evaluate the adsorption capacity of ImCON1 for $Cr_2O_7^{2-}$. As presented in Fig. S11,† the equilibrium adsorption capacities of $Cr_2O_7^{2-}$ at different concentrations were obtained. The isotherm was then fitted to the Langmuir model.

In addition to $Cr_2O_7^{2-}$ and CrO_4^{2-}, TcO_4^- ions are hazardous water pollutants because of the radioactivity of ^{99}Tc. Since handling radioactive species is inconvenient in a typical laboratory, we chose MnO_4^- as a non-radioactive surrogate for TcO_4^-. Mn and Tc are in the same periodic group, making MnO_4^- a close chemical analogue of TcO_4^-. Following the

methodology for $Cr_2O_7^{2-}$ and CrO_4^{2-} capture, we conducted detailed studies on removing MnO_4^- from water. The capture of MnO_4^- was monitored at $\lambda_{max} = 525$ nm. A rapid decline in the absorption spectrum was observed, and the purple solution was decolorised within 1 minute (Fig. 3c). Concurrently, the white solid adsorbent, ImCON1, turned dark brown. These dual observations strongly suggested an interaction between ImCON1 and permanganate ions (MnO_4^-). FT-IR analysis confirmed the presence of MnO_4^- in MnO_4^-@ImCON1, with the characteristic absorbance at 904 cm^{-1} (Fig. S6†). ImCON1 demonstrated highly promising results in the MnO_4^- sequestration from aqueous solutions. The uptake capacity reached 694.5 mg g^{-1}, significantly higher than those of previously reported compounds (Table S3†). To delve into the sorption rate of ImCON1 towards MnO_4^-, corresponding kinetic experiments were carried out. As illustrated in Fig. S9,† when the treatment duration was extended to 3 minutes, ImCON1 reduced the MnO_4^- concentration to below 54.5%. Further prolonging the treatment time beyond 2 minutes did not result in a significant decrease, indicating that the sorption process had reached equilibrium. The sorption kinetics of ImCON1 were further analysed by fitting the experimental data to a pseudo-second-order model (Fig. S12†). The high correlation coefficient obtained from the fitting suggests that the sorption process is likely governed by chemical adsorption. The ultrafast exchange kinetics can be primarily attributed to the small particle size, high porosity, and elevated positive charge density of ImCON1.

Given the harsh conditions of wastewater, the influence of pH on the sorption efficiency of oxo-anions was investigated. As illustrated in Fig. 3d, the impact of acid–base conditions on the sorption of CrO_4^{2-} was negligible. The removal efficiencies reached 100% within the pH range of 4 to 10. When ImCON1 was placed in a more acidic environment, specifically at pH 2, the removal percentage of CrO_4^{2-} decreased to 84%. In a strongly basic solution with a pH of 12, ImCON1 still demonstrated a high removal rate of 87% for CrO_4^{2-}. When contrasted with the results obtained for the removal of CrO_4^{2-}, the removal efficiency of $Cr_2O_7^{2-}$ was found to be relatively more significantly influenced by the basic environment at pH 12, as depicted in Fig. 3e. At pH 12, ImCON1 could achieve a removal rate of up to 84% for $Cr_2O_7^{2-}$. This phenomenon is likely attributed to different Cr(VI) ionic forms in aqueous solutions at various pH values. Furthermore, as presented in Fig. 3f, it was evident that the removal of MnO_4^- ions remained unaltered by the pH value. The demonstrated acid–base resistance of ImCON1 strongly suggests that the polymeric network featuring covalent linkers plays a crucial role in maintaining structural stability and enhancing the sorption capacity under harsh environmental conditions. To determine the chemical stability of ImCON1 in acidic and basic environments, samples of ImCON1 were suspended in 0.1 M HCl and 0.1 M NaOH solutions, respectively, for 24 hours. Fourier-Transform Infrared (FTIR) spectroscopy was utilised to analyse the samples. Under acidic conditions, as illustrated in Fig. S13,† the FTIR spectra of ImCON1 treated with HCl (blue curve) exhibit no significant shifts or disappearances of the characteristic peaks associated with the structure of pristine ImCON1 (pink curve). This observation indicates that the chemical bonds within ImCON1 remained largely intact under acidic conditions. Under basic conditions, the FTIR spectra of ImCON1 treated with NaOH (green curve) in Fig. S13† reveal certain alterations. Specifically, the frameworks of ImCON1 undergo a gradual loss of positive charges, which can be attributed to the deprotonation of C2–H from the imidazolium rings in basic solutions. Nevertheless, despite these modifications, the overall structure of ImCON1 retains a degree of stability, as the key characteristic peaks related to its primary framework can still be identified.

Wastewater contains competing anions (*e.g.*, F^-, Cl^-, Br^-, I^-, NO_3^-, SO_4^{2-}) and the target oxo-anions. Therefore, we conducted binary mixture studies for all oxo-anions with a 10-fold excess of moles of various competing anions. Notably, significant capture of the oxo-anions was still observed in the presence of competing anions. In the case of CrO_4^{2-} ions, efficient removal was achieved in the presence of F^-, Cl^-, Br^-, I^-, and NO_3^- ions, as shown in Fig. 3g. However, the removal efficiency for the SO_4^{2-}/CrO_4^{2-} ion mixture was relatively lower, reaching approximately 75%. Similar phenomena were also detected in the adsorption experiment of ImCON1 on the mixed solution containing $Cr_2O_7^{2-}$ (Fig. 3h). ImCON1 was able to capture over 84% of $Cr_2O_7^{2-}$ from the mixtures. This might be attributed to the high charge density of SO_4^{2-} ions and their strong interaction with the polymer network. Moreover, the removal of MnO_4^- ions remained unperturbed by other anions, as depicted in Fig. 3i. These binary mixture studies demonstrated the efficacy of ImCON1 in capturing oxo-anions, even when competing anions were present in the solution.

To study the effect of temperature on adsorption, we have investigated the capacities of ImCON1 for oxo-anions at different temperatures. As depicted in Fig. S14,† we systematically investigated the adsorption capacities of ImCON1 for CrO_4^{2-} ions across a range of temperatures. The results demonstrate that the adsorption capacity of ImCON1 for CrO_4^{2-} ions is temperature-dependent. Starting at 20 °C with an adsorption capacity of approximately 277 mg g^{-1}, the capacity steadily increased until it reached a peak value of 316.7 mg g^{-1} at 40 °C. Within this temperature interval, the enhancement in adsorption capacity upon increasing temperature is likely due to heightened molecular motion. This increased mobility promotes more effective interactions between ImCON1 and CrO_4^{2-} ions, facilitating adsorption. Conversely, as the temperature ascended beyond 40 °C (at 50 °C, 60 °C, and 70 °C), a decline in adsorption capacity was observed. This phenomenon can be ascribed to the elevated thermal energy at higher temperatures, which may induce the desorption of pre-adsorbed CrO_4^{2-} ions or disrupt the favourable binding interactions between the adsorbent (ImCON1) and the adsorbate (CrO_4^{2-} ions). Our research on the temperature-modulated adsorption of CrO_4^{2-} ions by ImCON1 reveals that an optimal temperature, around 40 °C in this context, can significantly enhance the adsorption capacity. In contrast, extremely low and high temperatures are detrimental to adsorption. These findings offer crucial insights for the practical application of

ImCON1 in removing oxo-anions under diverse thermal conditions.

Furthermore, an ImCON1-packed chromatographic column was fabricated and employed to remove oxo-anions from water. A 0.5 mM stock solution of each oxo-anion was passed through the column. A noticeable colour change in the eluent occurred for $Cr_2O_7^{2-}$, CrO_4^{2-}, and MnO_4^- ions, indicating their capture by ImCON1. UV-vis studies further confirmed the absence of $Cr_2O_7^{2-}$, CrO_4^{2-}, and MnO_4^- ions in the eluted water, demonstrating the utility of the ImCON1-based column for removing toxic oxo-anions (Fig. 4a, c and e). To determine whether the removal process within the column was anion exchange or surface adsorption, water was passed through the column loaded with oxo-anion@ImCON1. The colourless eluent verified the anion exchange mechanism, ruling out surface adsorption. Subsequently, the reusability of ImCON1 was investigated with a NaBr solution. When 0.5 M NaBr was passed through the column for $Cr_2O_7^{2-}$ and CrO_4^{2-}, a yellow solution emerged, indicating the presence of Cr(VI) oxo-anions. ImCON1 maintained its efficiency with no significant fluctuations over ten consecutive cycles (Fig. 4b, d and f). This study confirmed that ImCON1 remained stable after adsorbing the target oxo-anions and being regenerated with 0.5 M NaBr, enabling repeated capture of these anions across multiple cycles.

The validation of ImCON1's practical applicability holds substantial significance. Industrial wastewater samples laden with dichromate anions were procured from Dongzheng Chemical Co., Ltd in Shangnan County, Shaanxi Province, China. Before the adsorption experiment, a comprehensive compositional analysis of the wastewater was meticulously executed. The analysis revealed the presence of a diverse array of anions, including Cl^-, SO_4^{2-}, and NO_3^-, cations such as Na^+, Ca^{2+}, and Fe^{3+}, as well as organic substances. The wastewater exhibited a complex chemical makeup with a pH of approximately 6.5. Subsequently, adsorption experiments were conducted using ImCON1 in this industrial wastewater. The outcomes were remarkable. ImCON1 sustained a high adsorption rate for dichromate anions in this intricate wastewater milieu. The characteristic peak of $Cr_2O_7^{2-}$ in the wastewater solution at $\lambda_{max} = 362$ nm diminished rapidly. In a mere 30 seconds, approximately 82% of the chromate anions were removed, a performance comparable to that in pure synthetic solutions (Fig. S15†). The adsorption rate was scarcely influenced by the complex components present in the industrial wastewater. Regarding the saturated adsorption capacity, ImCON1 continued to showcase high-capacity adsorption performance. The saturated adsorption capacity for dichromate anions reached 331 mg g^{-1}. These findings unequivocally demonstrate that ImCON1 can efficiently sequester dichromate anions in industrial wastewater, thereby highlighting its outstanding adaptability and tangible practical value in real-world applications.

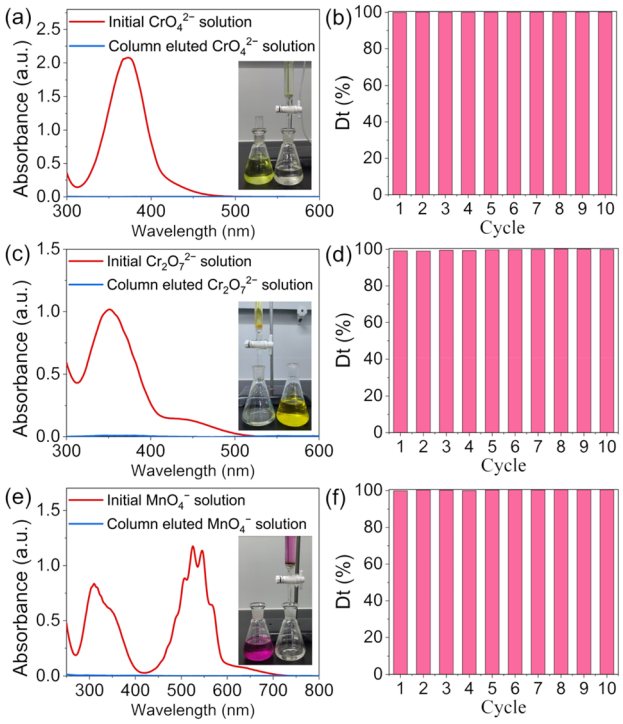

Fig. 4 Column adsorption experiments: UV-vis spectra for the solution of (a) CrO_4^{2-}, (c) $Cr_2O_7^{2-}$ and (e) MnO_4^- before and after passage through the column (inset: photograph of the column adsorption experiment for oxo-anion capture). Recyclability of ImCON1 for adsorption of (b) CrO_4^{2-}, (d) $Cr_2O_7^{2-}$ and (f) MnO_4^-.

Zeta potential provides crucial information about the surface charge of the material, which is closely related to its adsorption mechanism and stability in solution. We conducted zeta potential measurements on ImCON1 before and after the adsorption of $Cr_2O_7^{2-}$ (Fig. S16†). Before adsorption, the zeta potential of ImCON1 in an aqueous suspension was measured to be +25.4 mV at a pH of 7. This positive zeta potential is consistent with the cationic nature of ImCON1, as it contains positively charged imidazolium groups on its surface. The positive charge on the surface of ImCON1 is responsible for attracting the negatively charged toxic oxo-anions through electrostatic interactions, facilitating the adsorption process. After the adsorption of $Cr_2O_7^{2-}$, the zeta potential of ImCON1 decreased to +16.4 mV. This significant decrease in the zeta potential indicates that the negatively charged $Cr_2O_7^{2-}$ anions have been adsorbed onto the surface of ImCON1, neutralising a portion of the positive charge. The change in zeta potential also provides evidence for the anion-exchange mechanism, as the adsorbed anions alter the surface charge characteristics of the material. The change in zeta potential values of ImCON1 before and after adsorption of toxic oxo-anions indicates that the surface charge of ImCON1 is significantly affected by the adsorption process, and this change is directly related to the anion-exchange mechanism and the overall adsorption performance.

We employed Density Functional Theory (DFT) calculations to elucidate the adsorption mechanism of oxo-anions on ImCON1 comprehensively. The optimised structures depicted in Fig. S17† vividly illustrate the spatial configurations of ImCON1 before and after the adsorption of CrO_4^{2-}, $Cr_2O_7^{2-}$, and MnO_4^-. The specified distances, namely 2.116 Å for CrO_4^{2-}, 2.447 Å for $Cr_2O_7^{2-}$, and 3.133 Å for MnO_4^-, between the oxo-

anions and the ImCON1 framework, precisely quantify the proximity and potentially signify the interaction intensity. Simultaneously, Table S4† furnishes the sorbates' average isosteric heat and adsorption distances. The relatively elevated average isosteric heats, with values of 611.961 kcal mol^{-1} for CrO_4^{2-}, 609.029 kcal mol^{-1} for $Cr_2O_7^{2-}$, and 612.196 kcal mol^{-1} for MnO_4^-, strongly indicate an exothermic adsorption process. These DFT-generated structural and thermodynamic data synergistically complement our experimental findings, thereby establishing a robust theoretical framework for a profound understanding of the adsorption behaviour, including the high adsorption capacities and selectivities exhibited by ImCON1 towards oxo-anions.

Conclusions

In conclusion, we have successfully designed and synthesised a novel imidazolium-based cationic organic network, ImCON1. ImCON1 demonstrated outstanding performance in removing toxic oxo-anions. It had high adsorption capacities of 259 mg g^{-1} for CrO_4^{2-}, 1118 mg g^{-1} for $Cr_2O_7^{2-}$, and 694.5 mg g^{-1} for MnO_4^- (a surrogate for TcO_4^-), with ultra-fast kinetics following the pseudo-second-order model. The material exhibited excellent pH resistance, maintaining high removal efficiencies across a wide pH range. In the presence of competing anions, it still effectively captured the target oxo-anions. The ImCON1-packed chromatographic column efficiently removed oxo-anions *via* anion exchange and was reusable for at least ten cycles. The study on the temperature-dependent oxo-anion adsorption showed an optimal temperature of around 40 °C for maximum adsorption. DFT calculations provided insights into the adsorption mechanism, confirming an exothermic process. When applied to industrial wastewater containing dichromate anions, ImCON1 achieved a high adsorption rate (removing about 82% in 30 seconds) and a saturated adsorption capacity of 331 mg g^{-1}. Overall, ImCON1 shows great potential for wastewater treatment. Future work will focus on optimising its synthesis and exploring large-scale industrial applications.

Data availability

Data supporting the findings of this study, including all experimental data related to the synthesis, characterisation, and adsorption performance of ImCON1 such as FTIR, NMR, XPS, SEM, XRD, EDX mapping image, N_2 adsorption–desorption isotherm data, kinetic and isotherm data, are available in the paper and its ESI† and are available from the authors upon reasonable request.

Conflicts of interest

The authors declare that they have no conflict of interest.

Acknowledgements

This work was financially supported by the Natural Science Foundation of Shaanxi Province (2023-JC-QN-0100, 2024-JC-YBQN-0081), the Shaanxi Fundamental Science Research Project for Chemistry & Biology (22JHQ008), the Natural Science Foundation of Shangluo University (21SKY118), and the Youth Innovation Team of Shaanxi Universities.

References

1 M. A. Shannon, P. W. Bohn, M. Elimelech, J. G. Georgiadis, B. J. Mariñas and A. M. Mayes, *Nature*, 2008, **452**, 301–310.
2 J. Li, X. Dai, L. Zhu, C. Xu, D. Zhang, M. A. Silver, P. Li, L. Chen, Y. Li, D. Zuo, H. Zhang, C. Xiao, J. Chen, J. Diwu, O. K. Farha, T. E. Albrecht-Schmitt, Z. Chai and S. Wang, *Nat. Commun.*, 2018, **9**, 3007.
3 X. Yang, C. Yan, Z. Li, X. Li, Q. Yu, T. Sang, Y. Gai, Q. Zhang and K. Xiong, *Inorg. Chem.*, 2021, **60**, 5988–5995.
4 K. Kang, M. Zhang, L. Li, L. Lei and C. Xiao, *Ind. Eng. Chem. Res.*, 2022, **61**, 18870–18880.
5 Q. Li, M. Yi, L. Shao, Y. Kou, Y. Wei and K. Wang, *Sep. Purif. Technol.*, 2024, **350**, 127853.
6 A. Hassan, M. M. R. Mollah, R. Jayashree, A. Jain, S. Das and N. Das, *ACS Appl. Mater. Interfaces*, 2024, **16**, 24547–24561.
7 S. Jansone-Popova, A. Moinel, J. A. Schott, S. M. Mahurin, I. Popovs, G. M. Veith and B. A. Moyer, *Environ. Sci. Technol.*, 2019, **53**, 878–883.
8 M. Li, Z. Cui, S. Pang, L. Meng, D. Ma, Y. Li, Z. Shi and S. Feng, *J. Mater. Chem. C*, 2019, **7**, 11919–11925.
9 J. Chen, Y.-B. Wang, C. Ye, W. Lyu, J. Zhu, W. Yan and T. Qiu, *ACS Appl. Mater. Interfaces*, 2020, **12**, 28681–28691.
10 S. Das, G. Hazarika and D. Manna, *Chem.–Eur. J.*, 2023, **29**, e202203595.
11 S. Liu, L. Zhang, H. Kim, J. Sun and J. Yoon, *Coord. Chem. Rev.*, 2024, **501**, 215575.
12 *Perchlorate Environmental Contamination: Toxicological Review and Risk Characterization; Second External Review Draft, NCEA-1-0503*, U.S. EPA, Office of Research and Development, National Center for Environmental Assessment, U.S. Government Printing Office, Washington, DC, 2002.
13 B. K. Biswal and R. Balasubramanian, *J. Environ. Chem. Eng.*, 2023, **11**, 110986.
14 Y. Zhao, D. Kang, Z. Chen, J. Zhan and X. Wu, *Int. J. Electrochem. Sci.*, 2018, **13**, 1250–1259.
15 F. Liu, Y. Lou, F. Xia and B. Hu, *Chem. Eng. J.*, 2023, **454**, 140318.
16 S. Che, Z. Yang, I. Popovs, H. Luo, Y. Luo, W. Guo, H. Chen, T. Wang, K. Jie, C. Wang and S. Dai, *Chem. Commun.*, 2019, **55**, 13450–13453.
17 Y. Luo, Z. Yang, W. Guo, H. Chen, T. Wang, Y. Liu, Y. Lyu, H. Luo and S. Dai, *J. Mater. Chem. A*, 2020, **8**, 4740–4746.
18 Z.-J. Li, H.-D. Xue, Y.-Q. Zhang, H.-S. Hu and X.-D. Zheng, *New J. Chem.*, 2019, **43**, 11604–11609.
19 Z.-J. Li, H.-D. Xue, Y.-X. Ma, Q. Zhang, Y.-C. Li, M. Xie, H.-L. Qi and X.-D. Zheng, *ACS Appl. Mater. Interfaces*, 2019, **11**, 46197–46204.
20 S. Mollick, S. Fajal, S. Saurabh, D. Mahato and S. K. Ghosh, *ACS Cent. Sci.*, 2020, **6**, 1534–1541.

21 W. A. El-Mehalmey, A. H. Ibrahim, A. A. Abugable, M. H. Hassan, R. R. Haikal, S. G. Karakalos, O. Zaki and M. H. Alkordi, *J. Mater. Chem. A*, 2018, **6**, 2742–2751.
22 X. Jin, G.-Q. Wang, D. Ma, S.-Q. Deng, S.-L. Cai, J. Fan, W.-G. Zhang and S.-R. Zheng, *ACS Appl. Nano Mater.*, 2019, **2**, 5824–5832.
23 S. Q. Deng, X. J. Mo, S. R. Zheng, X. Jin, Y. Gao, S. L. Cai, J. Fan and W. G. Zhang, *Inorg. Chem.*, 2019, **58**, 2899–2909.
24 J. Liu, Y. Ye, X. Sun, B. Liu, G. Li, Z. Liang and Y. Liu, *J. Mater. Chem. A*, 2019, **7**, 16833–16841.
25 S.-Q. Deng, X.-J. Mo, S.-R. Zheng, X. Jin, Y. Gao, S.-L. Cai, J. Fan and W.-G. Zhang, *Inorg. Chem.*, 2019, **58**, 2899–2909.
26 Q. Sun, K. Yang, W. Ma, L. Zhang and G. Yuan, *Inorg. Chem. Front.*, 2020, **7**, 4387–4395.
27 D. Sheng, L. Zhu, C. Xu, C. Xiao, Y. Wang, Y. Wang, L. Chen, J. Diwu, J. Chen, Z. Chai, T. E. Albrecht-Schmitt and S. Wang, *Environ. Sci. Technol.*, 2017, **51**, 3471–3479.
28 S. Fajal, D. Ghosh, W. Mandal and S. K. Ghosh, *Chem. Commun.*, 2024, **60**, 1884–1887.
29 S. Dutta, S. Let, M. M. Shirolkar, A. V. Desai, P. Samanta, S. Fajal, Y. D. More and S. K. Ghosh, *Dalton Trans.*, 2021, **50**, 10133–10141.
30 K. Xiao, F. Xu, L. Jiang, N. Duan and S. Zheng, *Chem. Eng. J.*, 2016, **283**, 1349–1356.
31 S. Demirci, B. Ari, N. Aktas and N. Sahiner, *Front. Mater.*, 2022, **9**, 837701.
32 S. Fajal, S. Dutta and S. K. Ghosh, *Mater. Horiz.*, 2023, **10**, 4083–4138.
33 S. Dutta, A. Sinelshchikova, J. Andreo and S. Wuttke, *Nanoscale Horiz.*, 2024, **9**, 885–899.
34 R. Li, X. Tang, J. Wu, K. Zhang, Q. Zhang, J. Wang, J. Zheng, S. Zheng, J. Fan, W. Zhang, X. Li and S. Cai, *Chem. Eng. J.*, 2023, **464**, 142706.
35 S. Dutta, S. Fajal and S. K. Ghosh, *Acc. Chem. Res.*, 2024, **57**, 2546–2560.
36 A. Hassan, M. M. R. Mollah, S. Das and N. Das, *J. Mater. Chem. A*, 2023, **11**, 17226–17236.
37 S.-Y. Zhang, X.-H. Tang, Y.-L. Yan, S.-Q. Li, S. Zheng, J. Fan, X. Li, W.-G. Zhang and S. Cai, *ACS Macro Lett.*, 2021, **10**, 1590–1596.
38 C. Krishnaraj, H. S. Jena, K. Leus and P. V. D. Voort, *Green Chem.*, 2020, **22**, 1038–1071.
39 M. Debruyne, V. V. Speybroeck, P. V. D. Voort and C. V. Stevens, *Green Chem.*, 2021, **23**, 7361–7434.
40 J. Fan, X. Suo, T. Wang, Z. Wang, C.-L. Do-Thanh, S. M. Mahurin, T. Kobayashi, Z. Yang and S. Dai, *J. Mater. Chem. A*, 2022, **10**, 14310–14315.
41 E. Li, K. M. Siniard, Z. Yang and S. Dai, *Chem. Sci.*, 2024, **15**, 17720–17738.
42 K. Liu, Z. Xu, H. Huang, Y. Zhang, Y. Liu, Z. Qiu, M. Tong, Z. Long and G. Chen, *Green Chem.*, 2022, **24**, 136–141.
43 J. Zhao, G. Guo, D. Wang, H. Liu, Z. Zhang, L. Sun, N. Ding, Z. Li and Y. Zhao, *Green Chem.*, 2023, **25**, 3103–3110.
44 W. Song, Y. Tang, B. Y. Moon, Q. Liao, H. Xu, Q. Hou, H. Zhang, D.-G. Yu, Y. Liao and I. Kim, *Green Chem.*, 2024, **26**, 2476–2504.
45 Y. Chen, H. Chen, J. Jiang and H. Ji, *Green Chem.*, 2025, **27**, 1430–1439.
46 B. Aguila, Q. Sun, J. A. Perman, L. D. Earl, C. W. Abney, R. Elzein, R. Schlaf and S. Ma, *Adv. Mater.*, 2017, **29**, 1700665.
47 X. Shen, S. Ma, H. Xia, Z. Shi, Y. Mu and X. Liu, *J. Mater. Chem. A*, 2018, **6**, 20653–20658.
48 P. Samanta, P. Chandra, S. Dutta, A. V. Desai and S. K. Ghosh, *Chem. Sci.*, 2018, **9**, 7874–7881.
49 Y. Xie, J. Lin, H. Lin, Y. Jiang, J. Liang, H. Wang, S. Tu and J. Li, *J. Hazard. Mater.*, 2020, **392**, 122496.
50 Z.-J. Li, Q. Zhang, H.-D. Xue, X.-D. Zheng, H.-L. Qi and H.-C. Li, *Adv. Mater. Interfaces*, 2021, **8**, 2100016.
51 S. Mollick, S. Fajal, S. Saurabh, D. Mahato and S. K. Ghosh, *ACS Cent. Sci.*, 2020, **6**, 1534–1541.
52 Z.-J. Li, J.-Y. Liu, Y. Yu, K.-J. Chang, H. Wang, Y.-J. Li and K. Gai, *ACS Appl. Mater. Interfaces*, 2022, **14**, 23868–23876.
53 M. Zhu and Y. Yang, *Green Chem.*, 2024, **26**, 5022–5102.
54 A. Sen, S. Dutta, G. K. Dam, P. Samanta, S. Let, S. Sharma, M. M. Shirolkar and S. K. Ghosh, *Chem.–Eur. J.*, 2021, **27**, 13442–13449.
55 R. Li, K. Zhang, X. Yang, R. Xiao, Y. Xie, X. Tang, G. Miao, J. Fan, W. Zhang, S. Zheng and S. Cai, *Sep. Purif. Technol.*, 2024, **340**, 126765.
56 L. Zhai, S. Sun, P. Chen, Y. Zhang, Q. Sun, Q. Xu, Y. Wu, R. Nie, Z. Li and L. Mi, *Mater. Chem. Front.*, 2021, **5**, 5463–5470.
57 S. I. G. P. Mohamed, T. Zhang, Z. Jiang, A. M. Rappe and S. Nejati, *J. Phys. Chem. Lett.*, 2022, **13**, 10030–10034.
58 P. Zhang, Z. Wang, S. Wang, J. Wang, J. Liu, T. Wang, Y. Chen, P. Cheng and Z. Zhang, *Angew. Chem., Int. Ed.*, 2022, **61**, e202213247.
59 S. Chandra, A. Hassan, Prince, A. Alam and N. Das, *ACS Appl. Polym. Mater.*, 2022, **4**, 6630–6641.
60 L. Pan, Z. Liu, M. V. Hernandez, B. C. Schroeder, Y. Sun and C. F. J. Faul, *ACS Appl. Polym. Mater.*, 2024, **6**, 6416–6424.
61 Y.-S. Wang, X.-N. Yuan, X.-X. Gou, X.-T. Song, X. Wang, L. Guo, Y. Liu, C. Qiao, C. Zhou and Y.-F. Han, *Sci. China: Chem.*, 2025, **68**, 2478–2484.
62 X. Zhu, J. Han, Z. Chen, Z. Shi, J. Zhang and S. Guo, *Green Chem.*, 2024, **26**, 5339–5346.
63 S. Hao, Y. Liu, C. Shang, Z. Liang and J. Yu, *Polym. Chem.*, 2017, **8**, 1833–1839.
64 J. Li, D. Jia, Z. Guo, Y. Liu, Y. Lyu, Y. Zhou and J. Wang, *Green Chem.*, 2017, **19**, 2675–2686.
65 H. Pan, Z. Cheng, Z. Xiao, X. Li and R. Wang, *Adv. Funct. Mater.*, 2017, **27**, 1703936.
66 M. A. Ziaee, H. Zhong, C. Cui and R. Wang, *ACS Sustain. Chem. Eng.*, 2018, **6**, 10421–10428.
67 Y. Gong, H. Zhong, W. Liu, B. Zhang, S. Hu and R. Wang, *ACS Appl. Mater. Interfaces*, 2018, **10**, 776–786.